ORIGINAL RESEARCH

Tribological properties of 100% cellulose nanofiber (CNF) molding under dry- and boundary lubrication-conditions at CNF/steel contacts

H. Okubo · R. Nakae · D. Iba · K. Yamada · H. Hashiba · K. Nakano · K. Sato · S. Sasaki

Abstract Cellulose nanofibers (CNFs), which are plant-derived materials, have recently garnered considerable attention owing to their excellent mechanical properties, such as their low weight and high Young's modulus. Novel methods for producing 100% CNF bulk structural materials have been developed. However, the tribological properties of CNFs have not been investigated thus far although their mechanical properties are known and are comparable to those of some conventional structural materials. In this study, the tribological properties of a novel biomass material, 100% CNF molding, were investigated based on CNF/steel contacts under dry and boundary lubrication conditions at various temperatures. The friction test results showed that the friction coefficient and wear volume of the CNF molding increased with the test temperature of the CNF/steel tribopair under dry-sliding conditions. Conversely, no significant temperature dependence of the friction and wear properties was observed upon lubrication with a pure polyalfaolefin. The surface analytical results revealed that the amorphization of the CNF molding progressed on the worn surface, especially under dry-sliding conditions at a high temperature. All the results suggested that the friction and wear performance of the 100% CNF moldings strongly depends on the sliding test conditions, and the amorphization process of the CNF molding can affect its friction and wear performance.

Keywords Cellulose nanofiber · CNF · Boundary lubrication · Raman · AFM

H. Okubo (✉) · K. Nakano
Faculty of Environment and Information Sciences, Yokohama National University, 79-7 Tokiwadai, Hodogaya-ku, Yokohama 240-8501, Japan
e-mail: okubo-hikaru-xp@ynu.ac.jp

R. Nakae · D. Iba · K. Yamada
Department of Mechanical Engineering, Kyoto Institute of Technology, Goshokaidou-Chou Matsugasaki Sakyo-ku, Kyoto, Kyoto 606-8585, Japan

H. Hashiba
Chuetsu Pulp & Paper Co., Ltd., 282 Yonejima, Takaoka, Toyama 933-5833, Japan

K. Sato · S. Sasaki
Department of Mechanical Engineering, Tokyo University of Science, 6-3-1 Niijuku, Katsushika-ku, Tokyo 125-8585, Japan

Introduction

In recent years, there has been a need to reduce the environmental impact of industrial activities to implement sustainable development goals (SDGs). In this context, the development of biomass materials for industrial use has recently attracted attention as one of the major methods to solve environmental problems. Many research groups in the field of tribology have proposed biodegradable and bio-based tribo-materials (Wredenberg and Larsson 2009; Bustillos et al. 2018;

Bellemare et al. 2008; Nishitani et al. 2019). Several researchers have reported the tribological properties of polylactic acid (PLA), one of the most prevalent bridgeable polymers used as bulk plastic materials. The mechanical properties of PLA are inferior to those of the other polymeric materials used in industrial applications (Bustillos et al. 2018). To enhance the mechanical properties of PLA, additive-reinforced PLA composites have been fabricated, and their tribological properties have been investigated (Bellemare et al. 2008; Nishitani et al. 2019). Additive-reinforced PLA composites have several drawbacks, such as non-recyclability (owing to the presence of reinforced additives such as carbon fibers in PLA), relatively low glass-transition temperature, and low thermal dimensional stability, limiting the scope of their mechanical applications although the introduction of additive reinforcements can improve the wear resistance and friction properties of PLA. Moreover, the raw materials for manufacturing PLA are mainly derived from edible plants, which is a serious concern in the context of the global food crisis. Therefore, to expand the scope of biodegradable materials for tribological use, more studies are needed for the development of new bio-based tribological materials with enhanced mechanical properties, a higher glass-transition temperature, and higher thermal dimensional stability than those of the conventional bio-based materials; the use of inedible raw materials for the same is preferred.

Cellulose is one of the available bio-based polymers, and it plays an important role in the reinforcement of the cell wall of wood and plants (Posada et al. 2020; Elseify et al. 2019; Alexandrescu et al. 2013; Bondeson et al. 2006; Butchosa and Zhou 2014). Recently, cellulose nanofibers (CNFs), a plant-derived material with a diameter of a few nanometers, have attracted the attention of many researchers and engineers because of the following properties: (1) CNFs can be obtained from various inedible biomaterials such as plants and trees that are widely available, (2) CNFs are recyclable and biodegradable materials, and (3) CNFs have one-fifth the weight of steel, five times the Young's modulus of steel, and very low linear thermal expansion (high thermal dimensional stability) (Posada et al. 2020). CNFs can be derived from cellulose materials such as pulps treated by chemical and mechanical treatment processes, and they are typically obtained in the form of an aqueous dispersion

(Posada et al. 2020; Alexandrescu et al. 2013; Bondeson et al. 2006; Butchosa and Zhou 2014). In recent years, various industrial applications of CNFs have been developed, such as their use as a reinforcement fiber additive for plastic products, an insulator, a filter, and a viscosity improver for various products (Posada et al. 2020). The use of CNFs for tribological applications has been investigated in the tribological field. For one such application, CNFs and the other types of nanocellulose have been used as thickeners, viscosity improvers, and friction modifiers for water- and oil-based greases (Shariatzadeh and Grecov 2019; Gorbacheva et al. 2021; Zakani et al. 2022; Kinoshita et al. 2020). Kinoshita et al. reported that CNF-dispersed water has a large friction reduction effect on sliding systems at steel/steel contacts, and it was assumed that CNFs play a role as friction modifiers in water at the sliding contacts (Kinoshita et al. 2020). For another application, CNFs and natural fibers were used as reinforcement fibers to improve the mechanical and tribological properties of polymer composites (Barari et al. 2016; Shalwan and Yousif 2013; Omrani et al. 2016). These reports indicate that the tribological properties of the composites were improved by the addition of CNFs as the mechanical properties of the bulk polymer materials were enhanced. However, in a prior study, the tribological properties of such a CNF-reinforced polymer composite were dominated by the characteristics of bulk polymer materials since the concentration of the CNFs in the composites was low (approximately 1.0–10 wt.%) (Kinoshita et al. 2020). Moreover, the tribological properties of bulk CNFs remain unexplored although the CNFs have the potential to be used as a low-friction bulk material, according to the results of previous studies (Kinoshita et al. 2020; Barari et al. 2016).

Recently, methods have been developed for producing 100% CNF bulk structural materials, known as "100% CNF molding" (Chuetsu Pulp & Paper CO). The press-molding of CNF-dispersed water can yield CNF molding, and its mechanical properties are comparable to those of some conventional structural materials such as the engineering plastics PA66 and POM (approximate bending stress of 90–100 MPa), which have been used as tribological materials (Chuetsu Pulp & Paper CO). Moreover, it is well known that the CNFs have a higher glass-transition temperature (approximately 220 °C) and thermal dimensional stability (18 ppm/K) than conventional
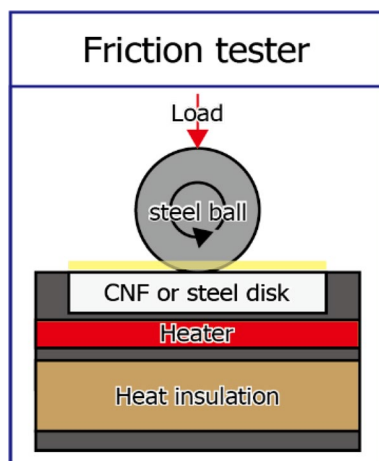
biomass materials. Hence, based on its mechanical and thermal properties, CNF molding has the potential for use as a mechanical element in tribological applications, such as in gears, bearings, and mechanical seals. However, the tribological properties of CNF molding have not been investigated thus far.

This study aims to investigate the lubrication performance and mechanisms of CNF moldings as a preliminary step toward expanding the application scope of CNF moldings to sliding components. In addition, by enhancing the functionality of CNF moldings, it aims to develop next-generation biomass sliding materials that can be applied to sliding mechanical elements. This study investigated the basic tribological properties of CNF moldings and the structural changes on the worn surfaces of the CNF moldings. The investigations were performed via friction tests of CNF/steel tribopairs using a ball-on disk tribotester under dry and boundary lubrication at different temperatures. Moreover, frictional surface characterization via SEM–EDS, Raman, and atomic force microscopy (AFM) was performed.

Test details

Materials and lubricants

A ball-on-disk-type friction tester was used for the friction test. Figure 1 shows the schematic diagram of the friction tester. A stepping motor rotates the ball, and the friction force between the rotating ball and fixed disk is measured by a load cell mounted beside the motor mounted on a liner guide. In the friction test, the coefficient of friction was obtained every 0.1 s, and the results were plotted to determine the friction behavior. The friction test was conducted at least three times. The friction test conditions are shown in Table 1.

A low-viscosity synthetic-base oil (polyalfaolefin 4: PAO 4, ISO viscosity grade:16) was used as the test lubricant. The ball (φ19.05 mm) specimen was made of SUJ2 bearing steel (Sa: 0.05 μm, nanoindentation hardness: 10 GPa). As the disk specimen (20×20 mm $\times$ t 5 mm), the CNF molding (nanoforest-CMB, density of 1.41 g/cm^3, Sa: 0.1 μm, nanoindentation hardness: 0.37 GPa, bending stress: 130 MPa) was prepared by press-molding a CNF water dispersion (aqueous counter collision method, nanoforest, Chuetu Pulp co., JP). Figure 2 shows the schematic of the preparation procedure of the CNF molding.

The nanoindentation hardness of the test specimen was measured using a Triboindenter (Ti950, Hysitrion, US). The CNF moldings used in this study were not subjected to any special surface treatment (such as water-resistant and functionalization). The degree of crystallinity of the CNF moldings was determined using an X-ray diffractometer (XRD, RINT-Ultima III, RIGAKU, JP) with Ni-filtered CuKα radiation at 40 kV and 30 mA. The scattered radiation was detected in the range of $2\theta = 5°$–$40°$.

To compare the tribological performance of the CNF molding and steel, a friction test was also conducted for a steel/steel tribopair, which used a SUJ2 steel ball and the disk (20×20 mm $\times$ t 5 mm, Sa: 0.05 μm, nanoindentation hardness: 10 GPa).

Fig. 1 Schematic diagram of the friction tester used in this study

Table 1 Friction test conditions

Applied load	10 N
Maximum Hertzian contact pressure	0.7 Gpa (steel/steel tribopair)
Sliding speed	0.01 m/s
Humidity	50–70%
Temperature	25, 50, 80 °C
Test duration	3600 s
Lubricated conditions	Dry/PAO 4
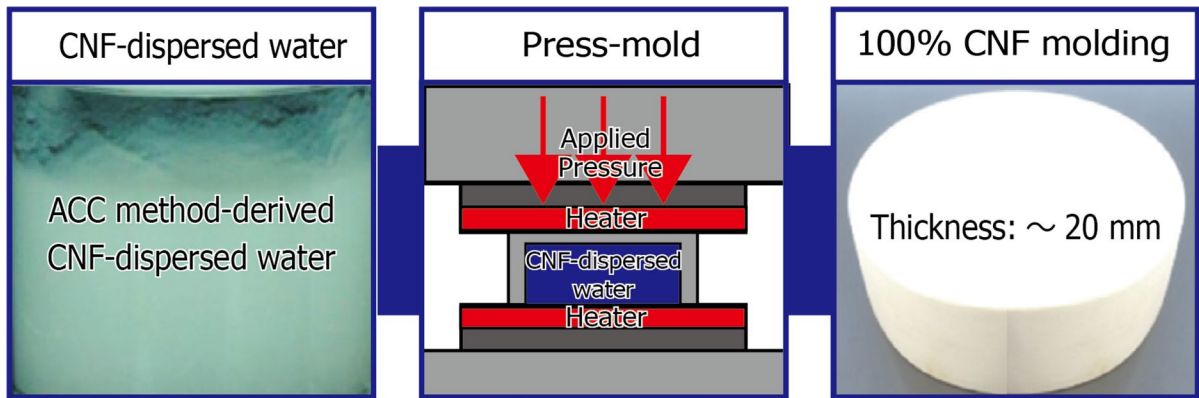
Fig. 2 Preparation procedure of the CNF molding

Surface analysis of the worn surface of the CNF molding was performed using a laser microscope (OLS5000, HITACHI, JP), SEM–EDS (Hitachi S3400 VPSEM and Inca EDX system, Japan, 15 kV accelerating voltage), Raman spectroscopy (LabRAM HR-800, HORIBA, JP), and AFM (AFM5100N/AFM5010 System, HITACHI, JP). For the Raman analysis, a laser wavelength of 633 nm was used to eliminate the influence of fluorescent components on the Raman spectrum.

Results

XRD results

Figure 3 shows the XRD pattern of the CNF moldings. The XRD pattern of the CNF moldings (Fig. 3) shows a peak at 2theta ~ 16.7°, which probably corresponds to the superimposed peaks related to (1–10) and (110) diffraction planes of cellulose I, and a peak at ~ 22.5° attributed to the (200) diffraction plane of cellulose I (French 2014).

The crystallinity index was calculated considering the peak intensity at 22.5°, and the intensity at the

Fig. 3 XRD pattern of the CNF molding
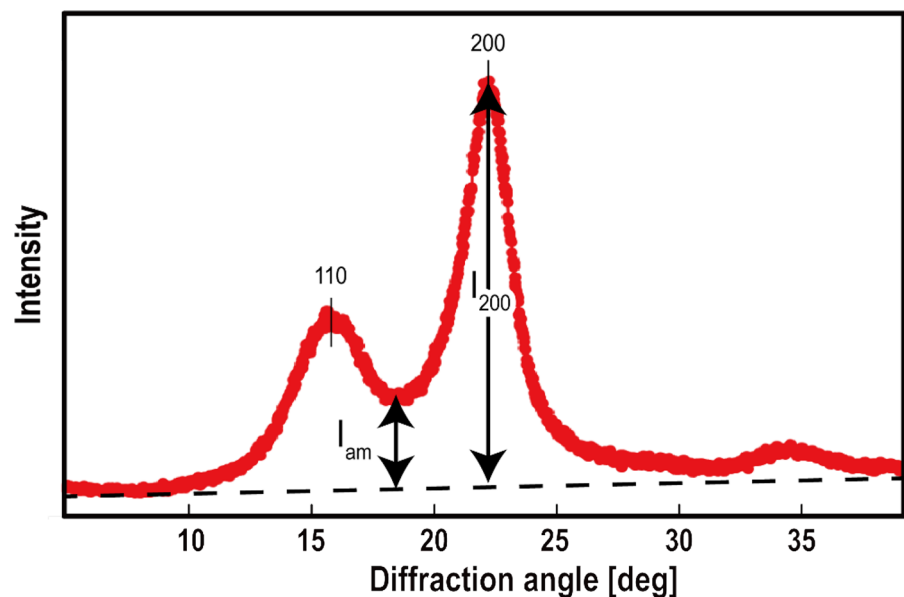
minimum between the 200 and 110 peaks, which corresponds to the intensity of the amorphous region at 18.5° (Segal et al. 1959; Nam et al. 2016):

$$\mathrm{CrI} = 100 \times \left(I_{200} - I_{am}\right) / \left(I_{200}\right)$$

where I_{200} is the height of the main peak (at about 22.5°) and I_{am} is the minimum in the intensity at about 18.5°. Based on the above, the crystallinity index of the CNF moldings was 75%.

Friction test results

Figure 4 shows the friction test results of the CNF/steel tribopairs at various temperatures under dry-sliding conditions. For test temperatures of 25 and 50 °C, the friction coefficient increased slowly initially (until 300 s) and then stabilized at ~ 300 s, and toward the end of the test, the friction coefficient was 0.13 and 0.24, respectively. Conversely, at 80 °C, the friction coefficient gradually increased from the initial period and finally stabilized in the range of 0.7–0.8 between 1800s and the end of the test. From the results, the temperature dependence of the frictional behavior of the CNF/steel tribopairs was observed under dry-sliding conditions. Figure 5 shows the friction test results of the CNF/steel tribopairs at various temperatures under lubrication with pure PAO 4. As seen, the friction coefficient gradually increased until 600 s and stabilized in the ~ 0.12–0.15 range, irrespective of the test temperature, after 600 s. This indicates that

temperature dependence was hardly observed under lubrication with pure PAO 4. Figure 6 shows the average friction coefficients of the CNF/steel and steel/steel tribopairs that were calculated by averaging the friction coefficient during the last 300 s in the test for each sliding condition. The CNF/steel tribopair exhibited a lower friction coefficient than the steel/steel tribopair, except for the dry-sliding condition at the test temperature of 80 °C. Notably, the CNF/steel tribopairs exhibited a 40% friction reduction effect for each condition under lubrication with pure PAO 4 compared to the steel/steel tribopair.

Figure 7 shows the optical microscope images of the wear tracks on the CNF molding and counterface steel ball for each sliding condition. Circular wear scars were observed for the CNF moldings, and there was no significant difference between the wear tracks on the CNF moldings and SUJ2 balls under all conditions, except for the dry-sliding condition at 80 °C. Conversely, for the same test temperature (80 °C), black tribofilms formed on the wear tracks of the CNF molding and steel balls under the dry-sliding condition. Therefore, it can be inferred that the black tribofilm formation is related to high-friction behavior, as shown in Fig. 4. Figure 8 shows the variation of the wear scar diameter for the disk and steel ball for the CNF/steel and steel/steel tribopairs at the end of the test for each sliding condition. Under dry-sliding conditions, the CNF/steel tribopair exhibited a lower wear scar diameter for the disk and wear width for
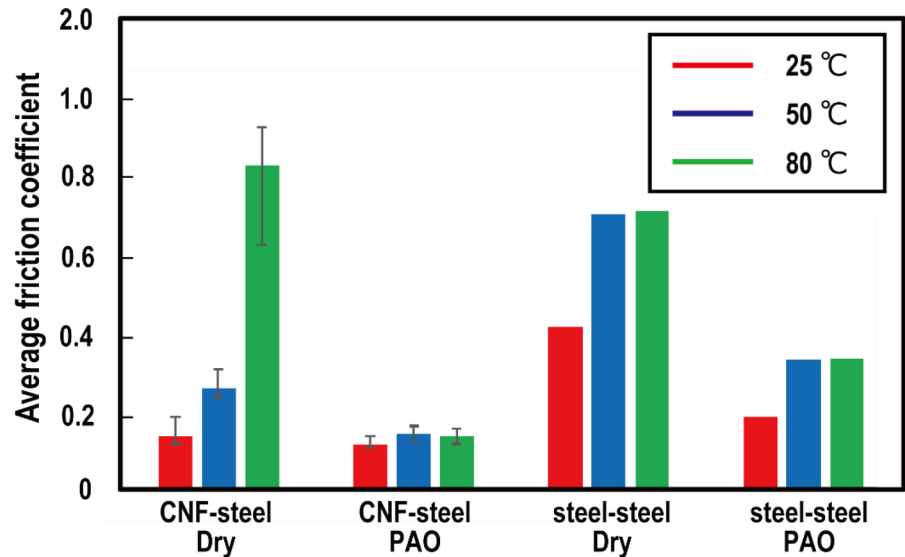

Fig. 4 Frictional behavior of the CNF/steel tribopairs under dry-sliding conditions with various temperatures
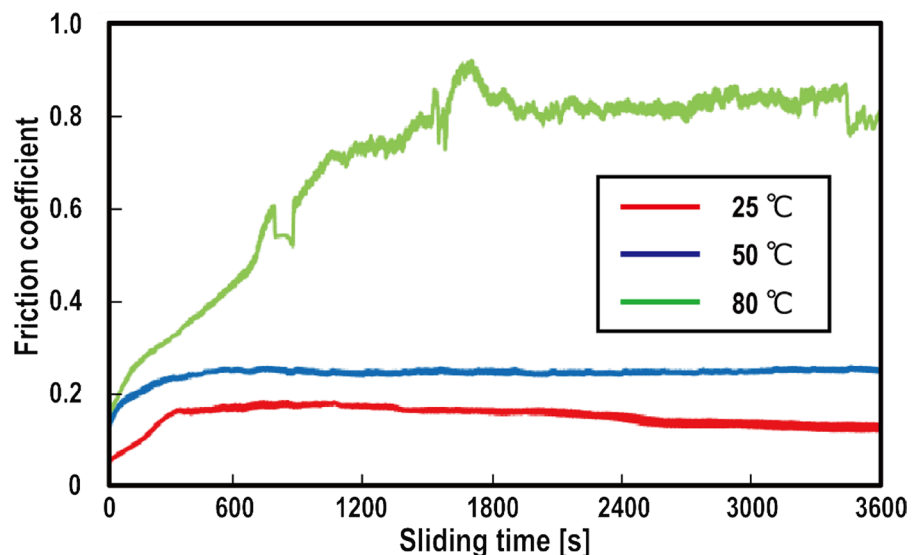
Fig. 5 Frictional behavior of the CNF/steel tribopairs under the lubrication with PAO 4 with various temperatures
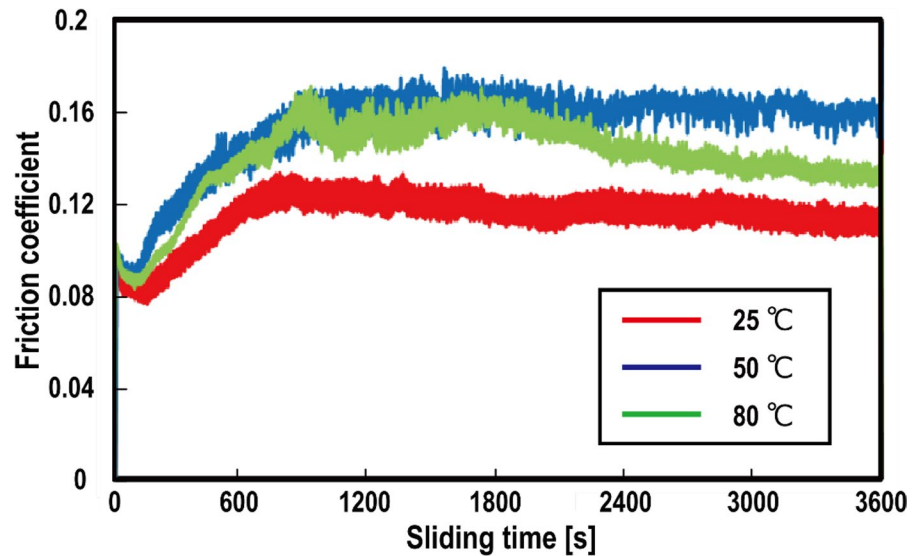
Fig. 6 Average friction coefficients of the CNF/steel and steel/steel tribopairs for each sliding condition

the ball than that for the steel/steel tribopair, except at 80 °C, where there was slight difference between the wear scar diameter and wear width for the CNF/steel and steel/steel tribopairs under the lubrication with pure PAO 4.

Based on the above observations, it can be concluded that the CNF molding exhibited a tribological performance comparable to that of the steel/steel tribopair under dry and boundary lubrication, except for the dry-sliding condition at the test temperature of 80 °C.

Worn surface analysis for the CNF molding

Normally, the structural changes in the tribo-materials strongly affect the tribological performance of the sliding system. Therefore, surface analysis was conducted on the worn surface of the CNF molding to understand its structure and determine the relationship between the friction and wear properties.

SEM–EDS

Figure 9 shows the SEM secondary electron (SE) images and EDS elemental maps of the as-molded and worn surfaces of the CNFs for each sliding condition. As can be seen in Fig. 9b, under dry conditions, the fraction of Fe increased with an increase in the test temperature (the red dots correspond to Fe in Fig. 9b). Conversely, this tendency was not observed for lubrication with pure PAO 4.

Figure 10 shows the atomic concentration of the elements on the worn surface of CNF for each sliding condition. Figure 10 also indicates that the concentration of Fe increased with an increase in the test temperature under dry-sliding conditions. Therefore, the iron-transfer film formed on the CNF molding and the transfer films might more easily form on the worn surface under higher temperatures.

Raman analysis

Figure 11 shows the optical images of the typical worn surfaces of the CNF disk. Two distinct regions were observed on the worn surface of the CNF disk: the red patchy regions surrounded by the red dotted lines and the other gray regions. Raman analysis was performed on the two regions. Figure 12 shows the Raman spectra of the as-molded CNF and the gray region on the worn surface, for each sliding condition. As seen, the peaks were observed at 320–370, 430, 500, 891, 990, 1057, 1090, 1377, 1406, 1458, and 1473 cm^{-1} and were assigned to CCC, CCO, CO ring deformation, CCC, CCO ring deformation, COC deformation glycosidic link, the vibration of the cellulose lateral unit at crystal regions, CH_2 deformation, CO_2 alcohol stretching, COC glycosidic link deformation and ring breathing symmetric stretching, HCC, HCO, COH, and CH_2 deformation, CH_2, HCC, HCO, and COH bending, CH_2, COH, and primary alcohol C_6OH bending, and deformation of CH_2, COH, and primary alcohol C_6OH. (Li and Renneckar 2011). In general, cellulose is known to be a naturally crystalline polymer, and its higher-order structure consists of a crystalline part with a regular arrangement and an amorphous part with a disordered structure. Moreover, it is known that Raman analysis can be used to evaluate the degree of crystallinity of cellulose based on several methods (Agarwal et al. 2010). In this study, the peak height (intensity) ratio of $I_{370}/$

I_{1057}, which is linearly proportional to the crystallinity value obtained via XRD, was used as the index of the crystallinity of the CNF molding (Agarwal et al. 2010). Figure 13 shows the peak height intensity ratio I_{370}/I_{1057} obtained from as-molded CNF and the worn surface of the CNF for each sliding condition. Notably, the worn surfaces showed a lower value of I_{370}/I_{1057} than the as-molded CNF. The value for the dry-sliding condition at 50 and 80 °C was one-fourth that of the as-molded CNF. From the results, it can be concluded that the amorphization of CNFs occurred at the sliding surfaces, and it could be promoted at higher temperatures under the dry-sliding condition.

Figure 14 shows the Raman spectra of the red patchy regions on the worn surface of the CNF molding for each sliding condition. As seen, magnetite- (Fe_3O_4, 538 and 670 cm^{-1}) and hematite- (Fe_2O_3, 225, 299, 613 cm^{-1}) derived peaks were observed (Lu and Tsai 2014). Figure 15 shows the Raman spectra of the bare and worn surfaces of the steel ball for each sliding condition. Only the peak of Fe_3O_4 was observed for all the cases, except for the dry-sliding condition at 80 °C which exhibited strong peaks that were assigned to both Fe_3O_4 and Fe_2O_3. This indicates that the iron oxide tribo-film, referred to as the "transfer film," mainly formed on the worn CNF surfaces, except for the dry-sliding condition at 80 °C. Therefore, it is concluded that the CNF transfer films were not present on the steel surface, as the CNF-derived peaks were not observed on the steel surface. Normally, the softer materials transfer to the harder materials at tribological contacts. However, in the case of the CNF/steel tribopair, steel was transferred to the CNF molding, although the hardness of the steel ball was much higher than that of the CNF molding. Therefore, it is inferred that the tribochemical reactions between the steel and CNF surfaces occurred at the sliding contacts, which promoted the formation of the transfer film on the CNF molding.

AFM analysis

In crystalline polymers, AFM phase imaging is useful for identifying the distribution of the crystalline and amorphous structures (Markey et al. 2001). Therefore, the AFM phase images of the as-molded CNF and the worn surface of the CNF moldings for each condition were obtained before and after the friction test to evaluate the details of the friction-induced
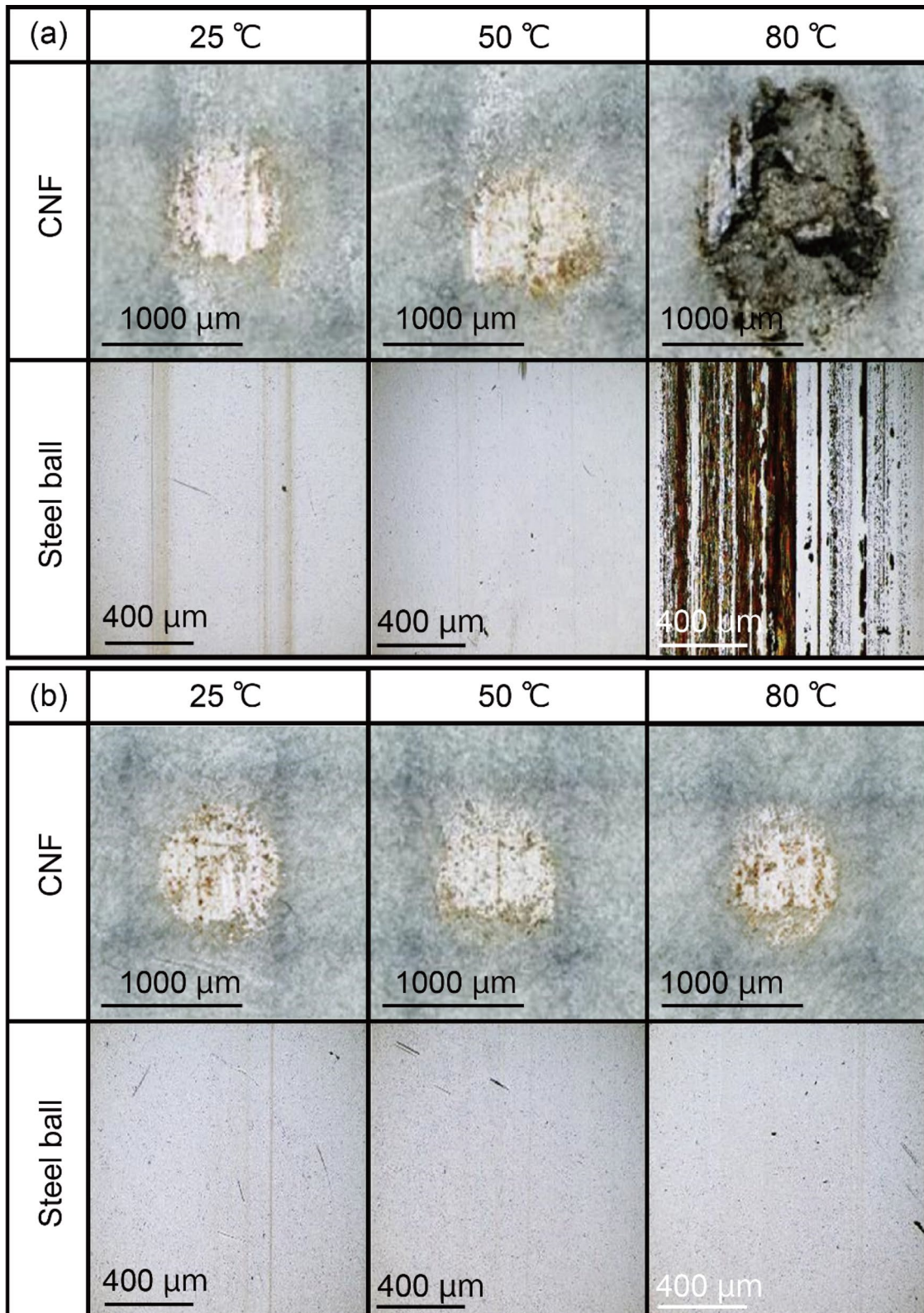
◄**Fig. 7** Optical microscope images of **a** the wear tracks on the CNF molding and **b** the counterface steel ball for each sliding condition

structural change in the CNF moldings. Figure 16 shows the AFM height and phase images of the as-molded and worn CNF surfaces of the CNF moldings. The surface roughness of CNF depended on the sliding conditions and increased with test temperature for both dry- and boundary lubrication conditions. In Fig. 16b, the brighter and darker regions correspond to the more elastic and viscous regions, respectively, indicating that the more elastic and viscous regions correspond to the crystalline and amorphous regions, respectively (Markey et al. 2001; Okubo and Yao 2021). As seen in Fig. 16b, comparing the images of the as-molded and the worn surfaces of CNF, the brighter regions were expanded for the worn surface of the CNF molding. This indicates that the amorphization of CNF proceeded on the worn surfaces. Moreover, from the AFM images, the lamellar size of the CNF molding can be estimated after the friction test, and it was found to be ~ 10–50 nm. Therefore, the CNF crystallinity regions can be collapsed by frictional energy, which results in a decrease in the lamellar size of the CNF molding on the worn surface.

Fig. 8 **a** Wear scar diameter of the disk and **b** wear scar width of the steel ball for the CNF/steel and steel/steel tribopairs at the end of the test for each sliding condition
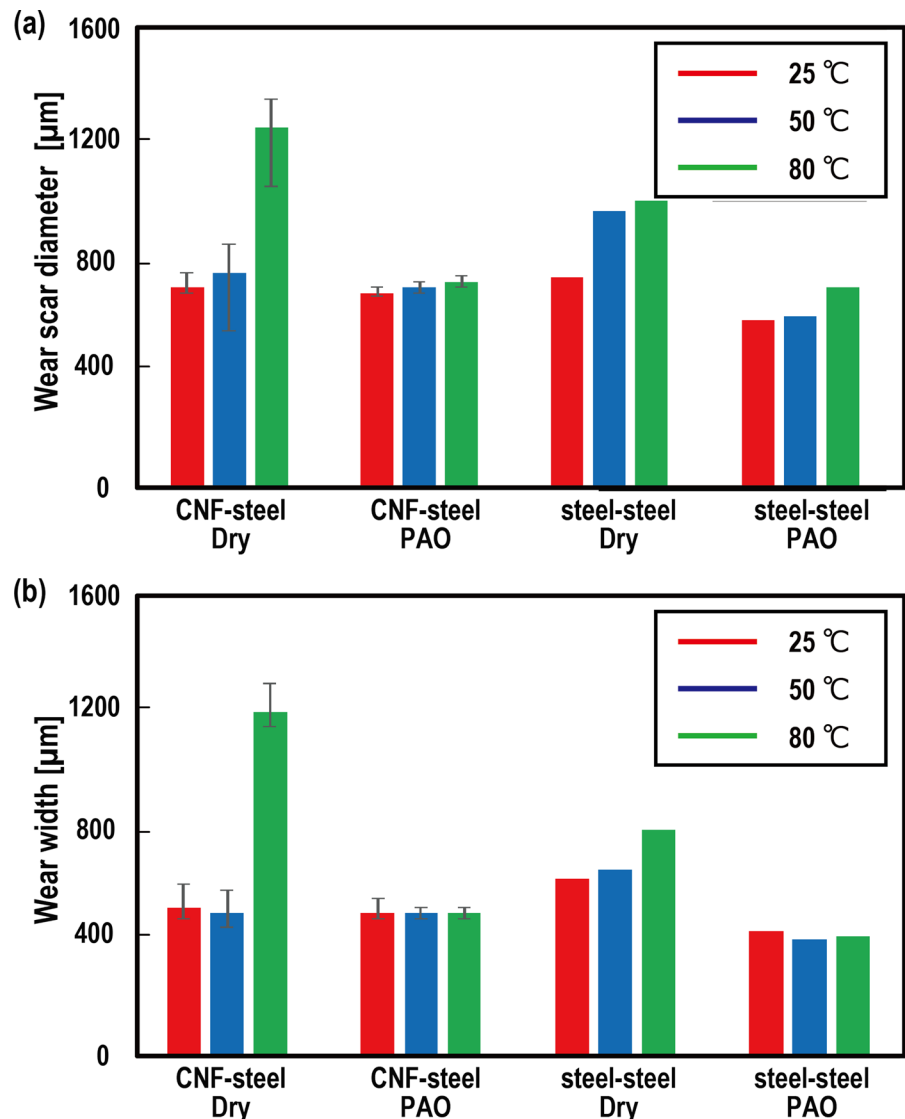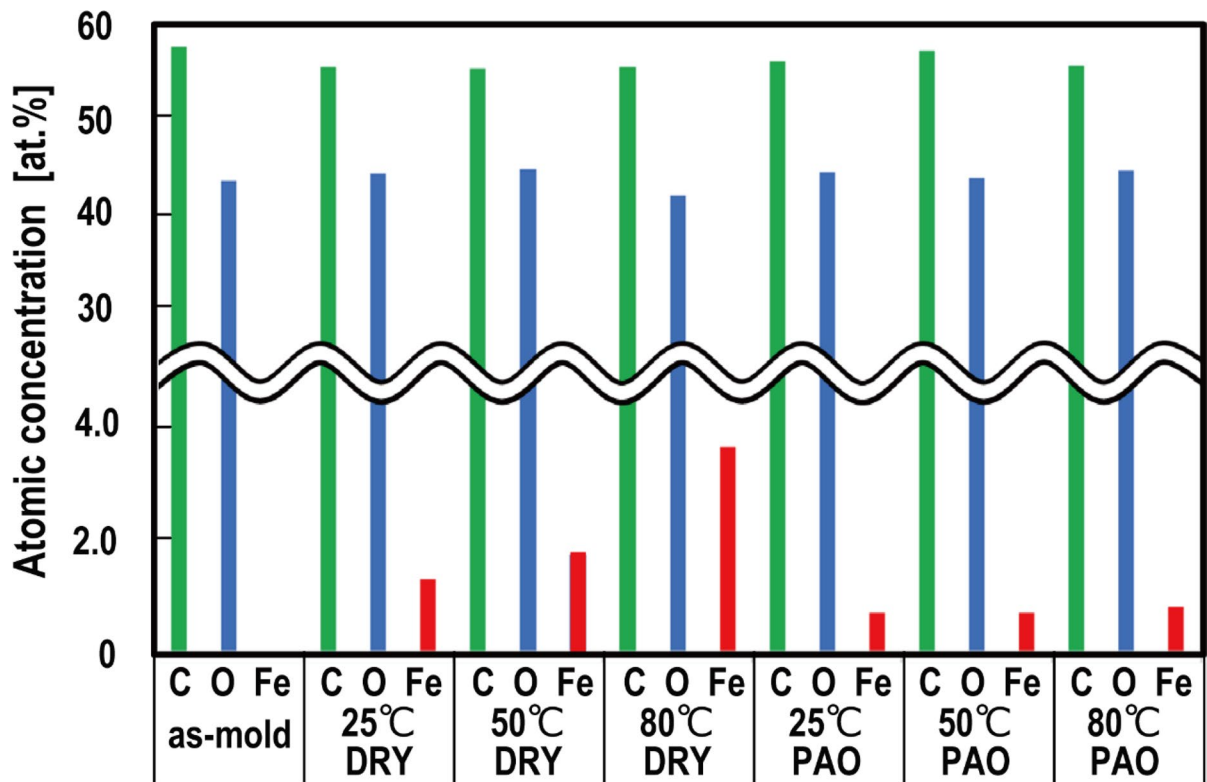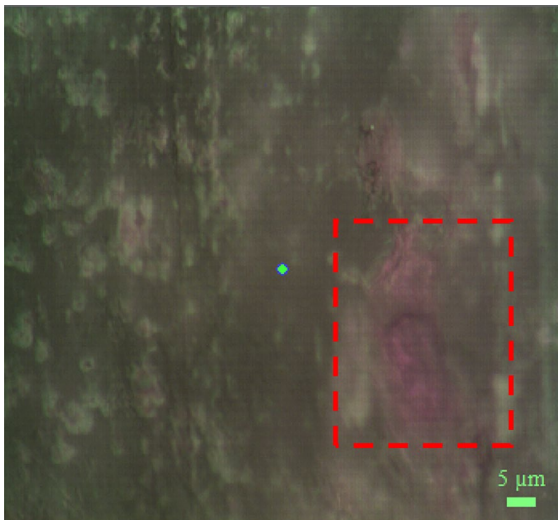
(a)
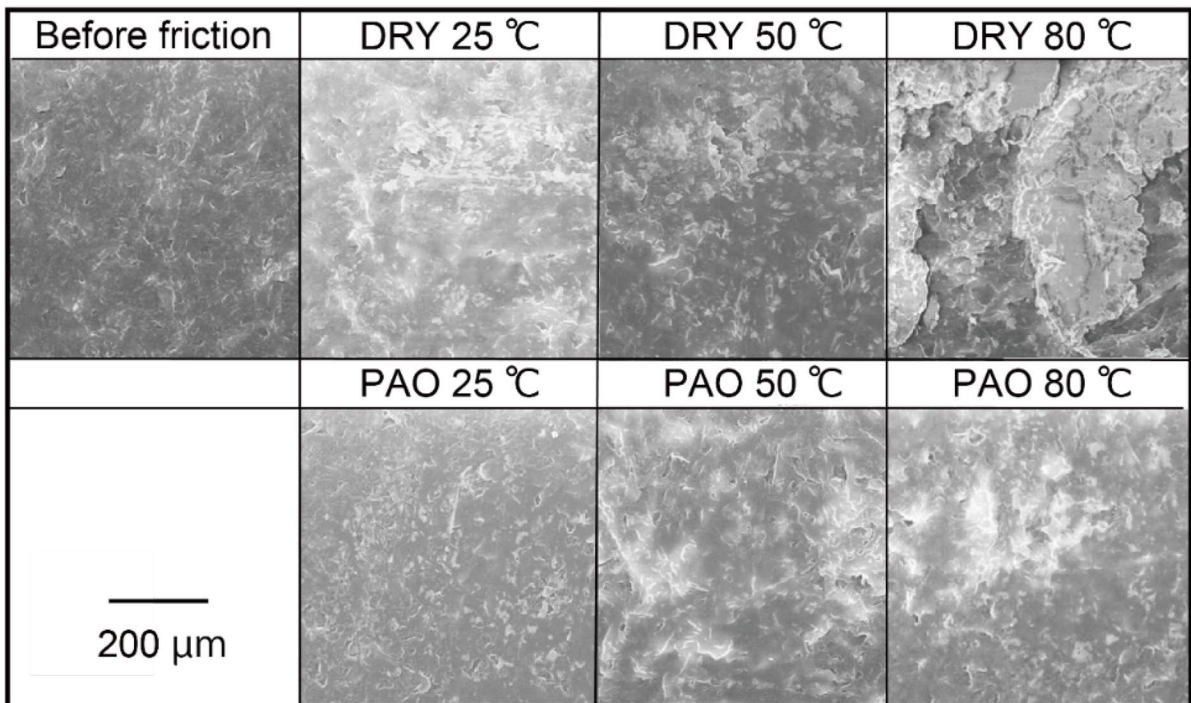
(b)
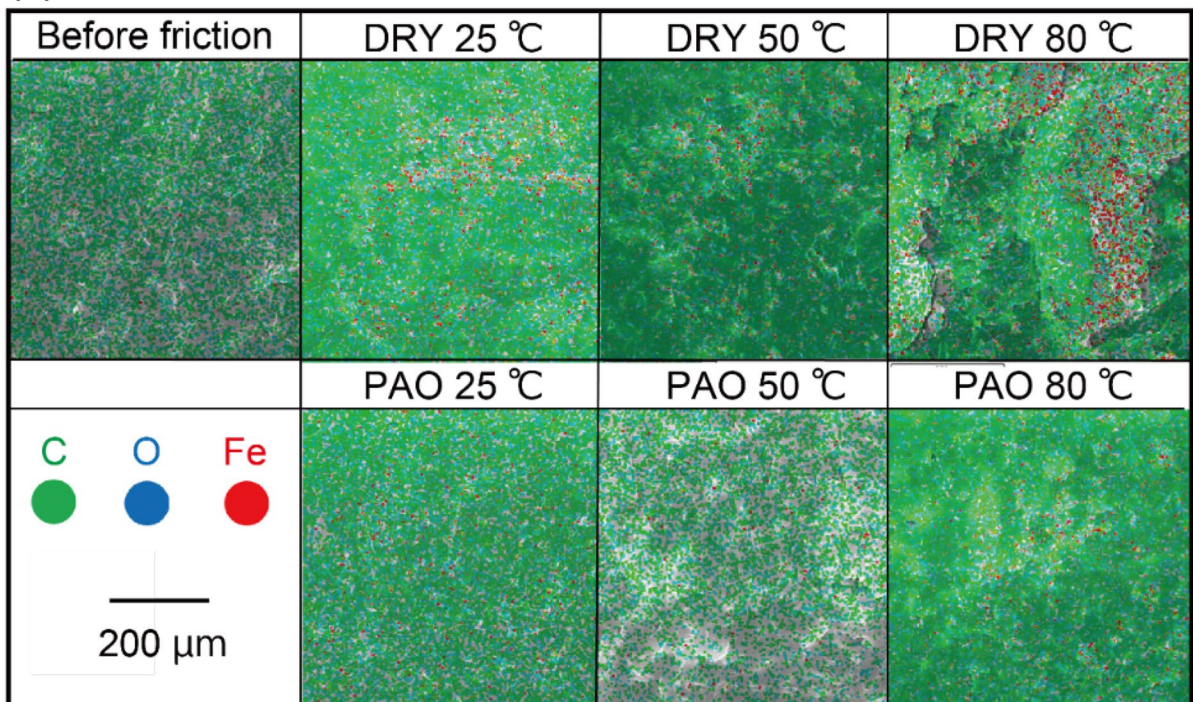
Fig. 9 **a** SEM secondary electron (SE) and **b** EDS element mapping images of the as-molded and worn CNF surfaces for each sliding condition

Fig. 10 Atomic concentration of various elements on the worn surface of the CNF for each sliding condition


Fig. 11 Optical images of the typical worn surfaces on the CNF disk

Discussion

This study investigated the fundamental tribological properties of CNF moldings and their structural changes in the worn surfaces. This section will discuss the relationship between the tribological properties, test temperature, and structural changes under dry and lubricated conditions.

Effect of test temperature and crystallinity on the tribological properties of the CNF molding

Figure 17 shows the relationship between the test temperature, average friction coefficient, and wear scar diameter on the CNF molding under dry-sliding conditions and lubrication with pure PAO. The friction coefficient and wear volumes of the CNF molding increased with the test temperature for the dry-sliding condition, such a temperature dependence was hardly observed under lubrication with pure PAO.
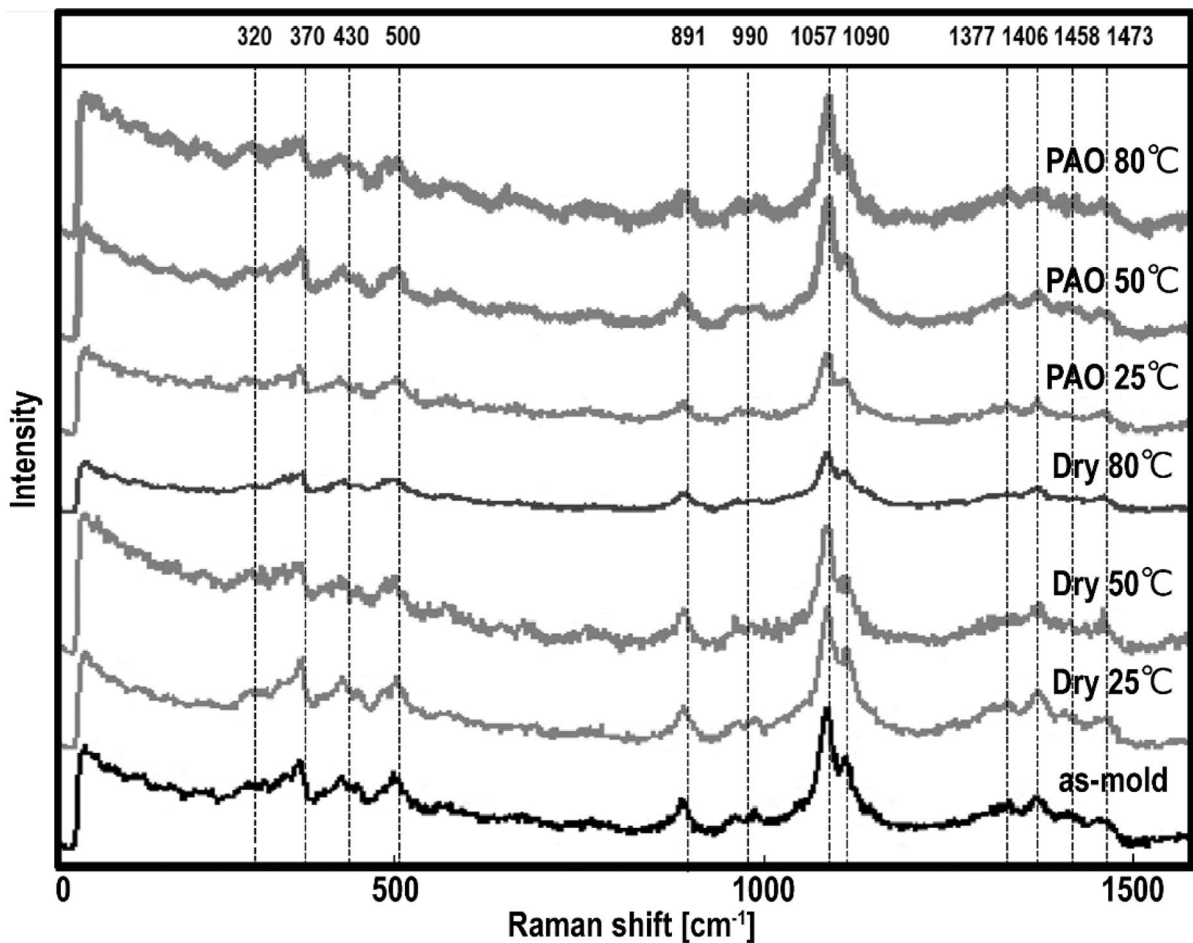
Fig. 12 Raman spectra of the as-molded CNF and the gray region on the worn surface for each sliding condition

Hence, the tribological properties of the CNF molding are strongly affected by the test temperature under the dry-sliding condition. This point will be discussed in the next section.

From the Raman results, the index I_{370}/I_{1057} indicated that the crystallinity of the CNF molding on the worn surface decreased after the sliding test and the degree of amorphization of the CNF molding depending on the sliding test conditions. Figure 18 shows the relationship between the average friction coefficient, the wear scar diameter of the CNF molding, and the intensity ratio I_{370}/I_{1057} for the dry condition and the condition of lubrication with pure PAO. Figure 18

shows that the friction coefficient and the wear scar diameter increased with a decrease in I_{370}/I_{1057}. This indicates that the crystallinity of the CNF molding on the sliding surface can affect its tribological properties. Such an amorphization of the worn surface of the CNF molding was also observed from the AFM results, as shown in Fig. 16b. The amorphization lowers the stiffness of crystallinity polymers. Therefore, friction-induced amorphization might also affect the stiffness of the worn surface of the CNF molding, affecting the tribological properties of the CNF molding. This point will be discussed in the next section.

Fig. 13 Peak height intensity ratio I_{370}/I_{1057} obtained from as-molded CNF and the worn surface of the CNF for each sliding condition
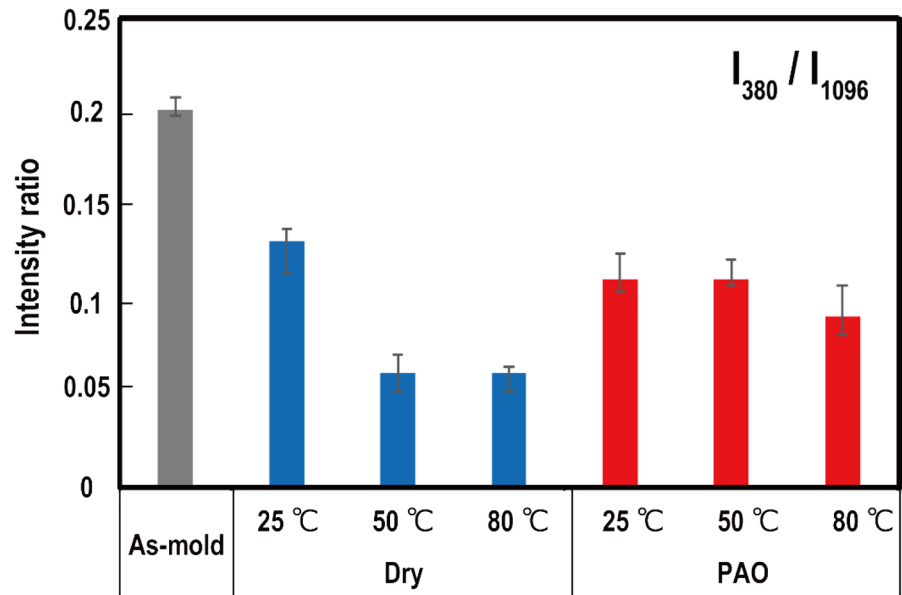
Fig. 14 Raman spectra at the red patchy regions on the worn surface of the CNF molding for each sliding condition
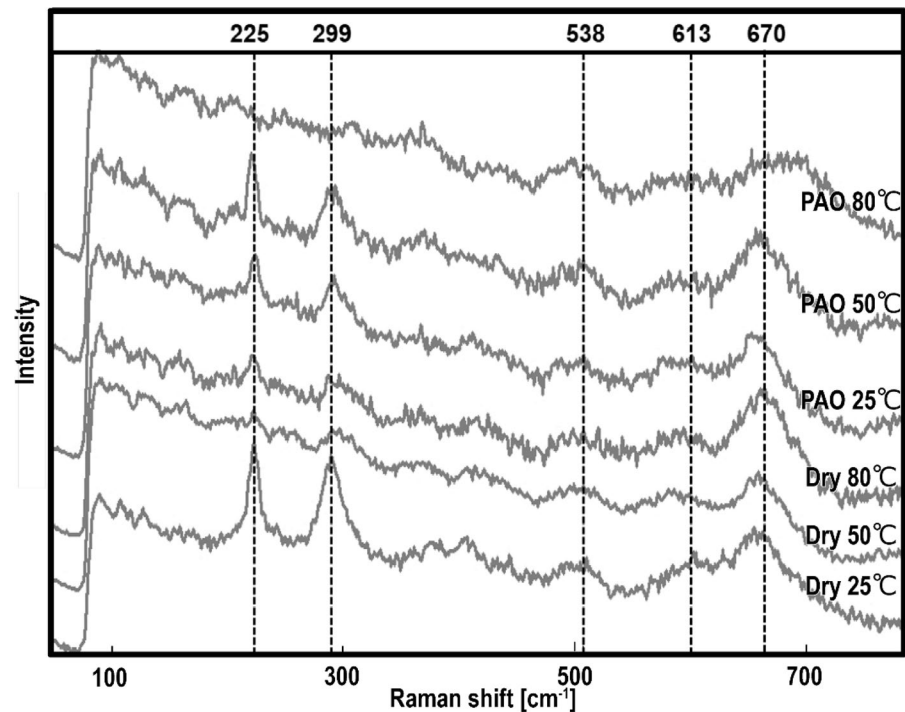

Wear mechanisms of the CNF molding

The friction and wear mechanisms of the CNF molding at the CNF/steel contacts are discussed in this section. Figure 19 shows the schematic diagram of the friction and wear mechanisms of the CNF/steel tribopairs under dry-sliding conditions. During the frictional process, tribochemical reactions between the CNF moldings and steel can occur at the CNF/steel tribological interface, as the formation of the

Fig. 15 Raman spectra of the bare surface and the worn surface of the steel ball for each sliding condition
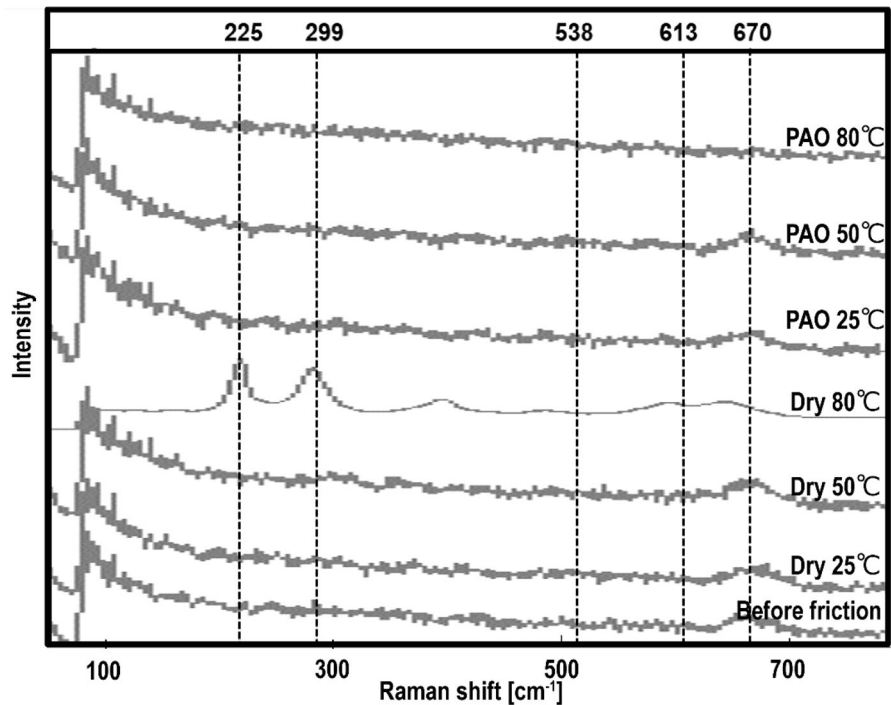
iron oxides on the CNF molding and steel surface was observed in the SEM–EDS and Raman results. Based on these results, it can be inferred that the hydroxy group on the CNF surfaces interacts with the iron surface during the frictional process, forming iron oxides on the worn surface of the CNF moldings. Subsequently, the tribochemical interaction and friction-induced thermal effects disrupt the crystalline structure of the CNF; in other words, they cleave the molecular chains of the CNFs at the contact region. Such amorphization lowers the stiffness of the CNF moldings at the contact region, promoting their wear. Based on the above hypothesis, the amorphization can easily progress for the high-temperature condition since the activation energy for the occurrence of the tribochemical reaction is lower at the contact region in this condition. Therefore, the wear of the CNF moldings increased with an increase in the test temperature and a decrease in their crystallinity under the dry-sliding conditions, as shown in Figs. 18 and 19.

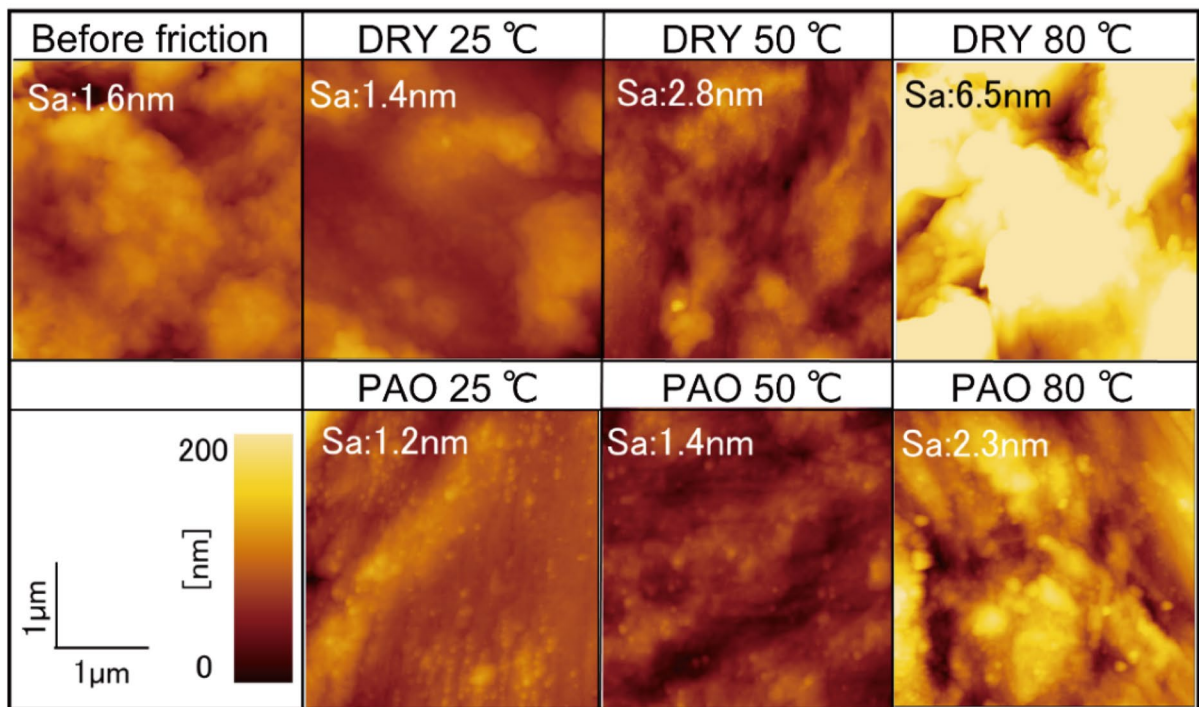Friction mechanisms of the CNF moldings

The temperature dependence of the frictional behavior of the CNF/steel tribopairs can also be explained by the tribochemical reactions at the frictional interface. At high temperatures, the formation of the iron oxides can progress rapidly on the CNF and steel surface. Such a tendency was observed from the analytical results for the test temperature of 80 °C, as shown in Figs. 7, 10, and 15. Therefore, the iron oxides cover the CNF molding and steel surface during the frictional process, and the configuration of the tribological contacts changes from the CNF/steel contacts to steel/steel (iron oxides) contacts, increasing the adhesion between the contact and the shear strength at the interface. For the lubrication with pure PAO, the above phenomena can be suppressed because the lubricant at the contacts can suppress the increment in the contact temperature, which is one of the driving forces for promoting the tribochemical reactions at the frictional interface.
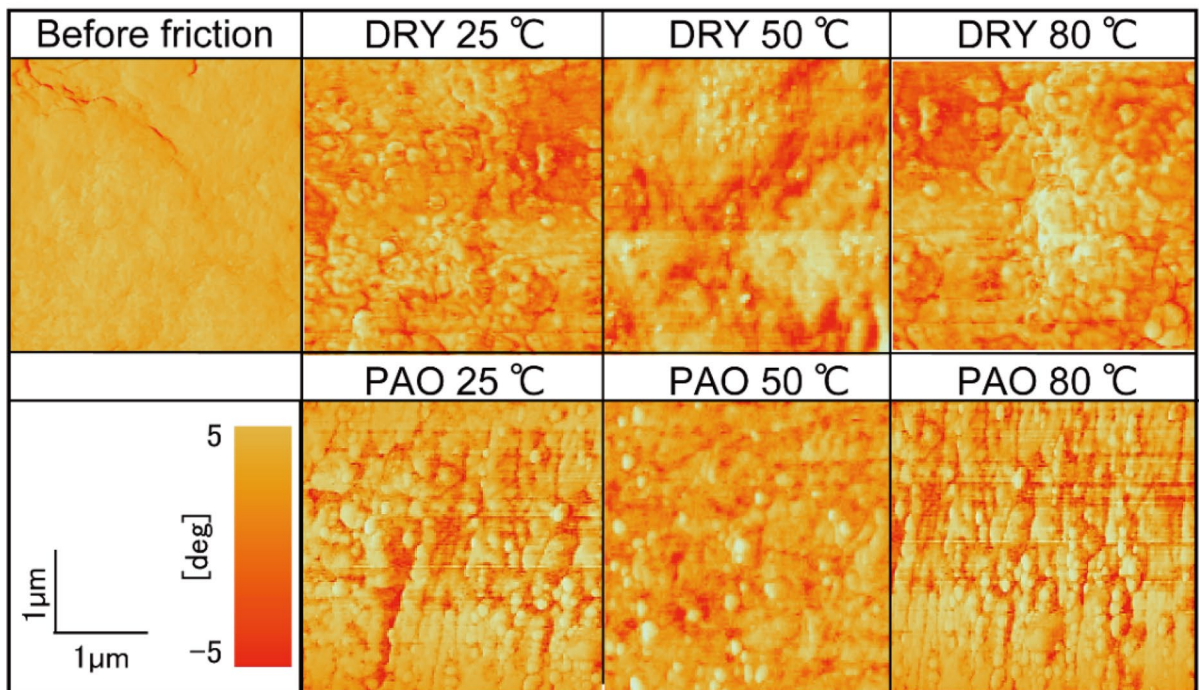
Conclusion

The tribological properties of 100% CNF moldings in CNF/steel tribopairs were investigated. The following results were obtained.
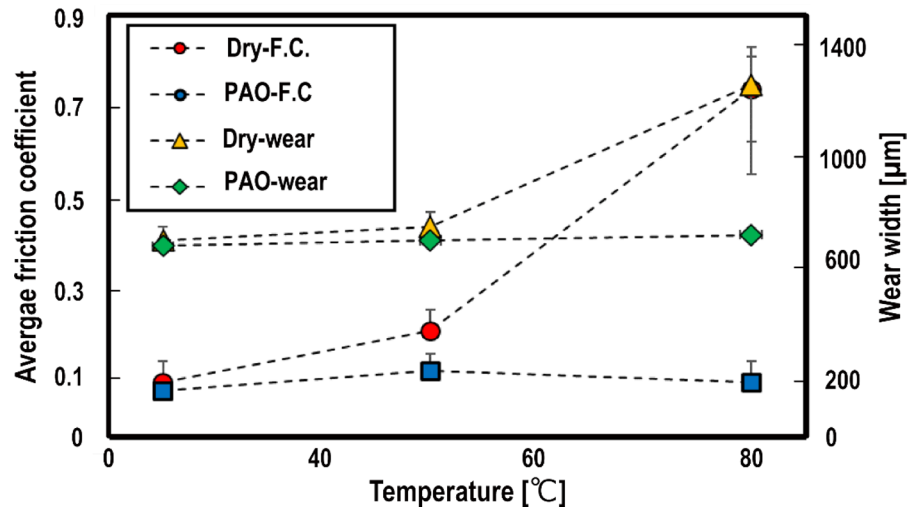
Fig. 16 **a** AFM height and **b** phase images of the as-molded CNF and the worn surface of the CNF moldings

Fig. 17 Relationship between the test temperature, the average friction coefficient, and the wear scar diameter on the CNF molding under the dry-sliding condition and lubrication with pure PAO

Fig. 18 Relationship between the average friction coefficient, the wear scar diameter of the CNF molding, and the intensity ratio I370/I1057 for the dry condition and lubrication with pure PAO
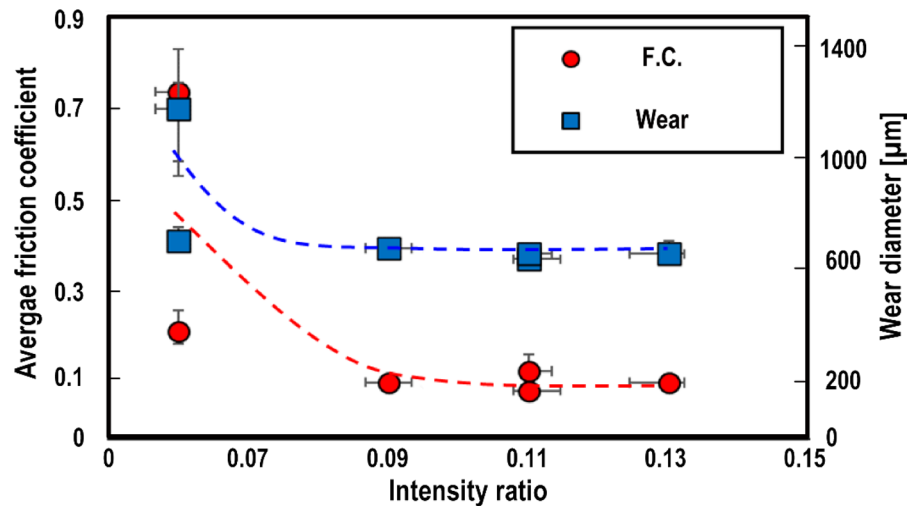
1. Under the dry-sliding conditions, the friction coefficient and wear volume of the CNF molding increased with the test temperature of the CNF/steel tribopair. Conversely, no significant temperature dependence of the friction and wear properties was observed in the case of lubrication with pure PAO.

2. The surface analysis showed that the cellulose crystalline structure of the CNF molding collapsed and amorphization progressed at the sliding contacts. The amorphous structural transformation was considerably prominent at high temperatures (50 °C, 80 °C) under the dry-sliding conditions.

3. The amorphization of the CNF moldings may be caused by the tribochemical interactions between the CNFs and steel surface, forming iron oxides at the CNF/steel contacts and resulting in friction-induced thermal effects. Moreover, such amorphization lowers the stiffness of the CNF moldings, resulting in the wear of the CNF moldings at the CNF/steel contact interface under the dry-sliding conditions.

In a future study, a critical comparison between CNF moldings and traditional sliding materials will be performed with regard to their life cycle, cost, and environmental impact.
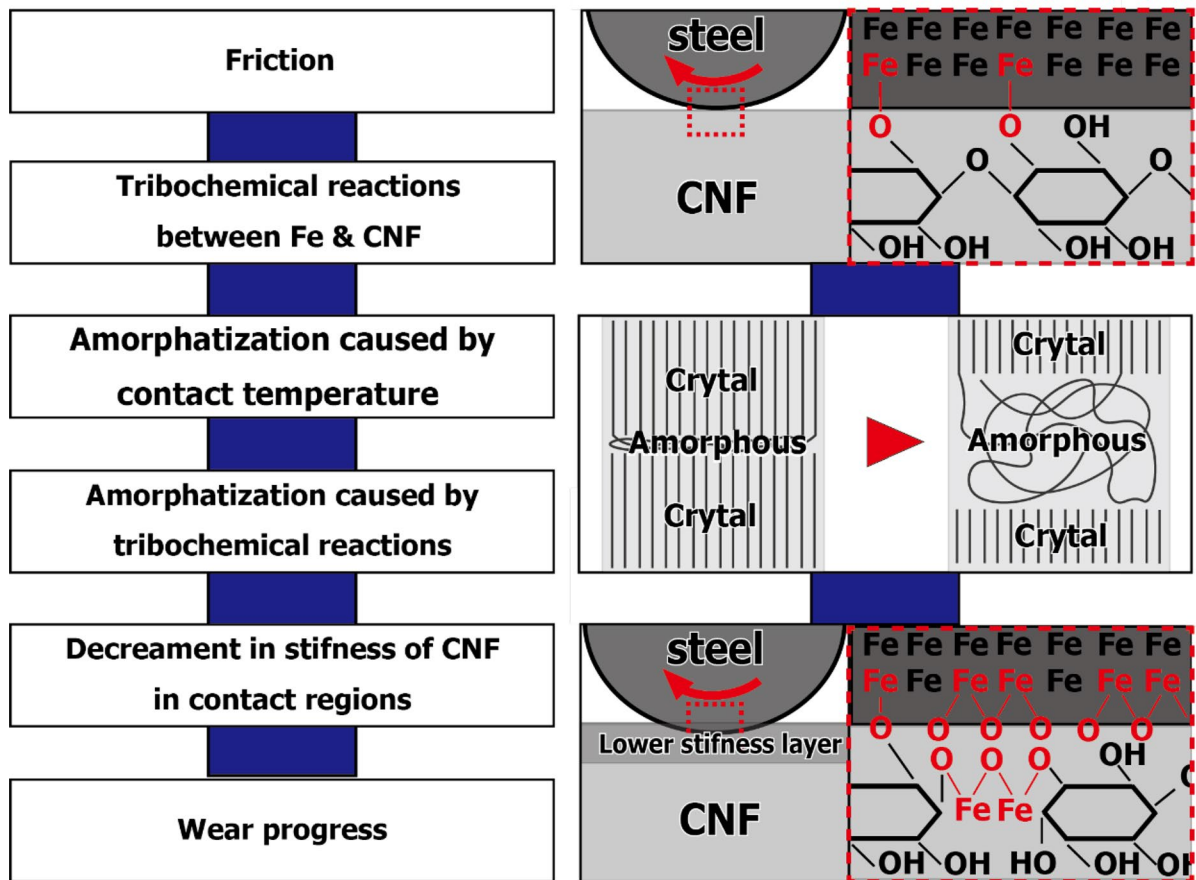
Fig. 19 Schematic diagram of the friction and wear mechanisms of CNF/steel tribopairs under dry-sliding conditions

Author contributions All authors contributed to the study conception and design. Material preparation, data collection, and analysis were performed by HO, RN, and HH. The first draft of the manuscript was written by HO, and all authors commented on previous versions of the manuscript. All authors read and approved the final manuscript.

Declarations

Competing interests The authors declare no competing interests.

Conflict of interest The authors have no relevant financial or non-financial interests to disclose.

Ethics approval and consent to participate Not applicable.

Consent for publication Not applicable.

Availability of data and materials The datasets used and/or analyzed during the current study are available from the corresponding author on reasonable request.

References

Agarwal UP, Reiner RS, Ralph SA (2010) Cellulose I crystallinity determination using FT–Raman spectroscopy: univariate and multivariate methods. Cellulose 17:721–733. https://doi.org/10.1007/s10570-010-9420-z

Alexandrescu L, Syverud K, Gatti A, Chinga-Carrasco G (2013) Cytotoxicity tests of cellulose nanofibril-based structures. Cellulose 20:1765–1775. https://doi.org/10.1007/s10570-013-9948-9

Barari B, Omrani E, Dorri Moghadam AD, Menezes PL, Pillai KM, Rohatgi PK (2016) Mechanical, physical and tribological characterization of nano-cellulose fibers reinforced bio-epoxy composites: an attempt to fabricate and scale the 'Green' composite. Carbohydr Polym 147:282–293. https://doi.org/10.1016/j.carbpol.2016.03.097

Bellemare SC, Dao M, Suresh S (2008) Effects of mechanical properties and surface friction on elastoplastic sliding contact. Mech Mater 40:206–219. https://doi.org/10.1016/j.mechmat.2007.07.006

Bondeson D, Mathew A, Oksman K (2006) Optimization of the isolation of nanocrystals from microcrystalline cellulose by acid hydrolysis. Cellulose 13:171–180. https://doi.org/10.1007/s10570-006-9061-4

Bustillos J, Montero D, Nautiyal P, Loganathan A, Boesl B, Agarwal A (2018) Integration of graphene in poly(lactic) acid by 3D printing to develop creep and wear-resistant hierarchical nanocomposites. Polym Compos 39:3877–3888. https://doi.org/10.1002/pc.24422

Butchosa N, Zhou Q (2014) Water redispersible cellulose nanofibrils adsorbed with carboxymethyl cellulose. Cellulose 21:4349–4358. https://doi.org/10.1007/s10570-014-0452-7

Elseify LA, Midani M, Shihata LA, El-Mously H (2019) Review on cellulosic fibers extracted from date palms (Phoenix dactylifera L.) and their applications. Cellulose 26:2209–2232. https://doi.org/10.1007/s10570-019-02259-6

Gorbacheva SN, Yadykova AY, Ilyin SO (2021) A novel method for producing cellulose nanoparticles and their application as thickeners for biodegradable low-temperature greases. Cellulose 28:10203–10219. https://doi.org/10.1007/s10570-021-04166-1

French AD (2014) Idealized powder diffraction patterns for cellulose polymorphs. Cellulose 21:885–896. https://doi.org/10.1007/s10570-013-0030-4

Kinoshita H, Inada Y, Matsumoto N (2020) Tribological property of cellulose nanofiber water dispersion using various material pairs. JAMDSM 14:JAMDSM0039. https://doi.org/10.1299/jamdsm.2020jamdsm0039

Li Q, Renneckar S (2011) Supramolecular structure characterization of molecularly thin cellulose I nanoparticles. Biomacromol 12:650–659. https://doi.org/10.1021/bm101315y

Lu JF, Tsai CJ (2014) Hydrothermal phase transformation of hematite to magnetite. Nanoscale Res Lett 9:230. https://doi.org/10.1186/1556-276X-9-230

Markey L, Janimak JJ, Stevens GC (2001) Modelling and simulation of the permanganic etching of banded spherulite polyethylene: correlation with AFM observations. Polymer 42:6221–6230. https://doi.org/10.1016/S0032-3861(01)00097-0

Nam S, French AD, Condon BD, Concha M (2016) Segal crystallinity index revisited by the simulation of X-ray diffraction patterns of cotton cellulose Iβ and cellulose II. Carbohydr Polym 135:1–9. https://doi.org/10.1016/j.carbpol.2015.08.035

Nishitani, Y., Sugawara, N., Kawasaki, K., Kajiyama, T. (2019). Tribological properties of Ureidosilane treated natural fiber reinforced plant-derived Polyamide1010 biomass composites Proceedings of PPS-33. In *AIP conference Proceedings*, vol. 2139, p. 120001 https://doi.org/10.1063/1.5121683.

Okubo H, Yao S (2021) Restoring mechanism of mechanical properties of recycled polyethylene pellet moldings by a repelletizing treatment using a twin-screw extruder. J Mater Cycles Waste Manag 23:1152–1176. https://doi.org/10.1007/s10163-021-01204-9

Omrani E, Menezes PL, Rohatgi PK (2016) State of the art on tribological behavior of polymer matrix composites reinforced with natural fibers in the green materials world. Eng Sci Technol an Int J 19:717–736. https://doi.org/10.1016/j.jestch.2015.10.007

Posada P, Velásquez-Cock J, Gómez-Hoyos C et al (2020) Drying and redispersion of plant cellulose nanofibers for industrial applications: a review. Cellulose 27:10649–10670. https://doi.org/10.1007/s10570-020-03348-7

Chuetsu Pulp & Paper CO, Nanoforest LTD Date of reading of 2022/06/16. https://www.chuetsu-pulp.co.jp/wordpress/wp-content/uploads/2021/05/nanoforest.pdf.

Segal L, Creely JJ, Martin AE, Conrad CM (1959) An empirical method for estimating the degree of crystallinity of native cellulose using the X-ray diffractometer. Text Res J 29:786–794. https://doi.org/10.1177/004051755902901003

Shalwan A, Yousif BF (2013) In state of art: mechanical and tribological behaviour of polymeric composites based on natural fibres. Mater Des 48:14–24. https://doi.org/10.1016/j.matdes.2012.07.014

Shariatzadeh M, Grecov D (2019) Aqueous suspensions of cellulose nanocrystals as water-based lubricants. Cellulose 26:4665–4677. https://doi.org/10.1007/s10570-019-02398-w

Wredenberg F, Larsson PL (2009) Scratch testing of metals and polymers: experiments and numerics. Wear 266:76–83. https://doi.org/10.1016/j.wear.2008.05.014

Yang YP, Zhang Y, Lang YX, Yu MH (2017) Structural ATR-IR analysis of cellulose fibers prepared from a NaOH complex aqueous solution. IOP Conference Series: Materials Science and Engineering 213:012039. https://doi.org/10.1088/1757-899X/213/1/012039

Zakani B, Salem H, Entezami S, Sedaghat A, Grecov D (2022) Effect of particle concentration on lubrication performance of cellulose nanocrystalline (CNC) water-based lubricants: mixed lubrication regime. Cellulose 29:3963–3984. https://doi.org/10.1007/s10570-022-04510-z